J|A|C|S
ARTICLES
Published on Web 11/08/2006

# Origin of the Linear Relationship between $CH_2$/NH/O−SWNT Reaction Energies and Sidewall Curvature: Armchair Nanotubes

Guishan Zheng,[‡] Zhi Wang, Stephan Irle,*[,†] and Keiji Morokuma*

*Contribution from the Cherry L. Emerson Center for Scientific Computation and Department of Chemistry, Emory University, Atlanta, Georgia 30322*

Received March 2, 2006; E-mail: sirle@emory.edu; morokuma@emory.edu

***Abstract:*** The origin of the linear relationship between the reaction energy of the $CH_2$/NH/O exo and endo additions to armchair (*n*, *n*) single-walled carbon nanotubes (SWNTs) and the inverse tube diameter (1/*d*) measuring sidewall curvature was elucidated using density functional theory and density functional tight binding methods for finite-size SWNT models with $n = 3, 4, ..., 13$. A nearly perfect linear relationship between $\Delta E$ and 1/*d* all through exohedral (positive curvature) and endohedral (negative curvature) additions is due to cancellation between the quadratic contributions of the SWNT deformation energy and the interaction energy (INT) between the deformed SWNT and $CH_2$/NH/O adducts. Energy decomposition analysis shows that the quadratic contributions in electrostatic, exchange, and orbital terms mostly cancel each other, making INT weakly quadratic, and that the linear 1/*d* dependence of INT, and therefore of $\Delta E$, is a reflection of the 1/*d* dependence of the back-donative orbital interaction of $b_1$ symmetry from the occupied $CH_2$/NH/O p$\pi$ orbital to the vacant C=C $\pi^*$ LUMO of the SWNT. We also discuss the origin of the two isomers (open and three-membered ring) of the exohedral addition product and explain the behavior of their associated minima on the C−C potential energy surfaces with changing *d*.

## 1. Introduction

The discovery of single-walled carbon nanotubes[1] (SWNTs) has spurred tremendous research activities[2] on how to employ these nowadays centimeter-long[3] molecules in nanomaterials applications, from the investigation and optimization of various formation mechanisms over purification[4,5] and functionalization[6−10] techniques to SWNT-based molecular engineering.[11] In particular, the electronic properties of these nanometer-size diameter tubes featuring a wide range of electrical conductivity (from semiconducting to metallic, dependent on the tube diameter and chirality[12−14] and functionalization[15,16]), combined with unique mechanical and thermal properties (unusual strength,[17] high thermal conductivity[18]) make SWNTs excellent candidates to either replace conventional materials in a wide variety of electronic devices or to allow the design of entirely new single-molecule-based devices. On the other end of the length spectrum, armchair SWNTs have been seriously suggested as a possible lightweight, cheap alternative for copper as a material to construct continent-spanning power transmission lines from solar farms or nuclear fusion reactors.[19,20]

Unfortunately, pure ("pristine") SWNTs usually form nanotube bundles due to their high polarizability, causing poor solubility and dispersion,[8] which poses many difficulties for their manipulation and processing and seriously limits their practical application. SWNT functionalization reactions of both covalent[6−9,21−23] (electronic structure and electrical conductivity

[‡] Current address: Department of Chemistry, University of Illinois at Urbana-Champaign, Urbana, IL 61801.

[†] Present address: Fukui Institute for Fundamental Chemistry, Kyoto University, Kyoto 606-8103, Japan.

(1) Iijima, S. *Nature* **1993**, *363*, 603−605.
(2) Dresselhaus, M. S.; Dresselhaus, G.; Avouris, P. *Carbon nanotubes: Synthesis, Structure, Properties and Applications*; Spinger-Verlag: Heidelberg, Germany, 2001; Vol. 80.
(3) Zheng, L. X.; O'Connell, M. J.; Doorn, S. K.; Liao, X. Z.; Zhao, Y. H.; Akhadov, E. A.; Hoffbauer, M. A.; Roop, B. J.; Jia, Q. X.; Dye, R. C.; Peterson, D. E.; Huang, S. M.; Liu, J.; Zhu, Y. T. *Nat. Mater.* **2004**, *3*, 673−676.
(4) Dailly, A. Y., J. W. L.; Ahn, C. C.; Miura, E.; Yazami, R.; Fultz, B. *Appl. Phys. A* **2005**, *A80*, 717−722.
(5) Mallikarjuna, N. N.; Manohar, S. K.; Aminabhavi, T. M. *Polym. News* **2005**, *30*, 6−13.
(6) Strano, M. S.; Dyke, C. A.; Usrey, M. L.; Barone, P. W.; Allen, M. J.; Shan, H.; Kittrell, C.; Hauge, R. H.; Tour, J. M.; Smalley, R. E. *Science* **2003**, *301*, 1519−1522.
(7) Banerjee, S.; Hemraj-Benny, T.; Wong, S. S. *Adv. Mater.* **2005**, *17*, 17−29.
(8) Dyke, C. A.; Tour, J. M. *J. Phys. Chem. A* **2004**, *181*, 11151−11159.
(9) Banerjee, S.; Wong, S. S. *J. Phys. Chem. B* **2002**, *106*, 12144−12151.
(10) Niyogi, S.; Hamon, M. A.; Hu, H.; Zhao, B.; Bhowmik, P.; Sen, R.; Itkis, M. E.; Haddon, R. C. *Acc. Chem. Res.* **2002**, *35*, 1105−1113.
(11) Solares, S. D.; Blanco, M.; Goddard, W. A., III. *Nanotechnology* **2004**, *15*, 1404−1415.
(12) White, C. T.; Mintmire, J. W. *J. Phys. Chem. B* **2004**, *109*, 52−65.
(13) Joselevich, E. *ChemPhysChem* **2004**, *5*, 619−624.
(14) Anantram, M. P. *Appl. Phys. Lett.* **2001**, *78*, 2055−2057.
(15) Collins, P. G.; Bradley, K.; Ishigami, M.; Zettl, A. *Science* **2000**, *287*, 1801−1804.
(16) Kong, J.; Franklin, N. R.; Zhou, C.; Chapline, M. G.; Peng, S.; Cho, K.; Dai, H. *Science* **2000**, *287*, 622−625.
(17) Wong, E. W.; Sheehan, P. E.; Lieber, C. M. *Science* **1997**, *277*, 1972−1975.
(18) Hone, J.; Whitney, M.; Piskoti, C.; Zettl, A. *Phys. Rev. B* **1999**, *59*, R2514−R2516.
(19) Smalley, R. E. 2nd NASA-Rice Workshop on SWNT Nucleation and Growth Mechanisms, Boerne, TX, 2005.
(20) Smalley, R. E.; Colbert, D. T.; Dai, H.; Liu, J.; Rinzler, A. G.; Hafner, J. H.; Smith, K.; Ting, G.; Thess, A. PCT Int. Appl., 1998; p 126.
(21) Mickelson, E. T.; Huffman, C. B.; Rinzler, A. G.; Smalley, R. E.; Hauge, R. H.; Margrave, J. L. *Chem. Phys. Lett.* **1998**, *296*, 188−194.

modifying[6,15,24]) and $\pi$ stacking[25,26] (electronic structure preserving) types have become popular for improving SWNT solubility and hence processability[8] and may also become very important in tethering SWNTs to surfaces and nanostructures.[7] Moreover, it was discovered recently that metallic and semiconducting SWNTs give rise to different thermodynamic reactivities toward chemical addition reactions,[6,27] which allows them to be separated[7,28−31] and spectroscopically characterized.[32−34]

Despite the obvious importance of covalent SWNT functionalization reactions, detailed atomic level understanding about the structural and electronic defects created by these reactions is still lacking. In particular, we do not know how exactly covalent functional groups are incorporated into the $\pi$-conjugated carbon network of the SWNT sidewalls, although it is clear that $sp^3$ hybridization, vacancy, and Stone−Wales-type defects are most likely somehow involved in defect creation.[35] Experimentally, no method is capable of providing atomistically resolved structural data of functionalization defects, although it has recently become possible to quantify[36] and characterize sidewall-attached functional groups themselves,[33,34,37,38] and it was also experimentally found that small-diameter tubes (SDNTs) are more reactive toward oxidation than large-diameter tubes.[39−41] Despite this progress, virtually nothing is known for certain about the molecular and electronic structures of functionalization-induced defects created on the tube sidewall carbon network.

Theoretical exploration is a natural complementary approach to such investigations, and exohedral SWNT functionalization has been widely studied using integrated ONIOM and QM/MM approaches[42−44] as well as pure density functional theory (DFT)[28,30,45−58] and density functional tight binding (DFTB) calculations.[55] A well-defined problem easily accessible to theoretical investigations is the effect of curvature on the reactivity of the SWNTs, and it was found previously[47−49,52,54−58] that the total reaction energy $\Delta E$ for the exohedral SWNT addition of addend X

$$\Delta E(\mathrm{X-SWNT}) = E(\mathrm{X-SWNT}) - E(\mathrm{X}) - E(\mathrm{SWNT}) \quad (1)$$

shows a decreasing trend with increasing $d$. This behavior was explained by the larger pyramidalization angle[59] of SDNT carbon atoms,[56] which are already more susceptible to adapt $sp^3$ configuration than those of large-diameter tubes. In addition, a greater strain energy in the case of SDNTs is released by breaking the central $C_a-C_a$ bond, stabilizing the reaction product.[60] In more quantitative studies, it was found that the total reaction energy $\Delta E$ of exohedral addition products depends linearly on the reciprocal tube diameter $d$ for X = H and Al atoms[47] and X = $NH_2$[52] according to

$$\Delta E = \Delta E_0 + C/d \quad (2)$$

based on generalized gradient approximation (GGA) DFT calculations with periodic boundaries. The binding energy (BE) these authors are referring to is simply defined as $-\Delta E$ from eq 1. The Gülseren and Zhao groups suggested that $\Delta E_0$ is a quantity related solely to the adatom/electrophilic agent and corresponds to its reaction (=negative binding) energy on a planar graphite surface ($1/d = 0$, which is equivalent to $n = \infty$) and that $C$ is a constant related to the tube itself according to ref 47. One of the factors determining $C$ is apparently related to tube chirality: Gülseren et al. determined $C$ to be −144.8 (kcal·Å)/mol for zigzag SWNTs independent of the electrophile, whereas Zhao et al. found $C$ to be −114.2 (kcal·Å)/mol for a series of armchair SWNTs. While both groups noticed the linear relationship between $\Delta E$ and $1/d$, they did not give a satisfactory quantitative explanation for this finding besides a general statement on s−p mixing.[47] Kudin et al. have investigated in detail the $1/d^2$ behavior of the sidewall deformation energy and investigated fluorination energies and energy cancellation of the


(22) Kim, K. S.; Park, K. A.; Kim, H. J.; Bae, D. J.; Lim, S. C.; Lee, Y. H.; Kim, J. R.; Kim, J.-J. *J. Korean Phys. Soc.* **2003**, *42*, S137−S142.
(23) Kuzmany, H.; Kukovecz, A.; Simon, F.; Holzweber, M.; Kramberger, C.; Pichler, T. *Synth. Met.* **2004**, *141*, 113−122.
(24) Kudin, K. N.; Bettinger, H. F.; Scuseria, G. E. *Phys. Rev. B* **2001**, *63*, 045413/1−045413/4.
(25) Chen, R. J.; Zhang, Y.; Wang, D.; Dai, H. *J. Am. Chem. Soc.* **2001**, *123*, 3838−3839.
(26) Chen, J.; Collier, C. P. *J. Phys. Chem. B* **2005**, *109*, 7605−7609.
(27) Miyata, Y.; Mania, Y.; Kataura, H. *J. Phys. Chem. B* **2006**, *110*, 25−29.
(28) Chen, Z.; Du, X.; Du, M.-H.; Rancken, C. D.; Cheng, H.-P.; Rinzler, A. G. *J. Am. Chem. Soc.* **2003**, *3*, 1245−1249.
(29) Chattopadhyay, D.; Galeska, I.; Papadimitrakopoulos, F. *J. Am. Chem. Soc.* **2004**, *125*, 3370−3375.
(30) Maeda, Y.; Kimura, S.-i.; Kanda, M.; Hirashima, Y.; Hasegawa, T.; Wakahara, T.; Lian, Y.; Nakahodo, T.; Tsuchiya, T.; Akasaka, T.; Lu, J.; Zhang, X.; Gao, Y.; Yu, Y.; Nagase, S.; Kazaoui, S.; Minami, N.; Shimizu, T.; Tokumoto, H.; Saito, R. *J. Am. Chem. Soc.* **2005**, *127*, 10287−10290.
(31) Kim, S. N.; Luo, Z.; Papadimitrakopoulos, F. *Nano Lett.* **2005**, *5*, 2500−2504.
(32) Brar, V. W.; Samsonidze, G. G.; Santos, A. P.; Chou, S. G.; Chattopadhyay, D.; Kim, S. N.; Papadimitrakopoulos, F.; Zheng, M.; Jagota, A.; Onoa, G. B.; Swan, A. K.; Uenlue, M. S.; Goldberg, B. B.; Dresselhaus, G.; Dresselhaus, M. S. *J. Nanosci. Nanotechnol.* **2005**, *5*, 209−228.
(33) Kim, U. J.; Liu, X. M.; Furtado, C. A.; Chen, G.; Saito, R.; Jiang, J.; Dresselhaus, M. S.; Eklund, P. C. *Phys. Rev. Lett.* **2005**, *95*, 157402/1−157402/4.
(34) Kim, U. J.; Furtado, C. A.; Liu, X.; Chen, G.; Eklund, P. C. *J. Am. Chem. Soc.* **2005**, *127*, 15437−15445.
(35) Hirsch, A. *Angew. Chem., Int. Ed.* **2002**, *41*, 1853−1959.
(36) Kuznetsova, A.; Mawhinney, D. B.; Naumenko, V.; Yates, J. T., Jr.; Liu, J.; Smalley, R. E. *Chem. Phys. Lett.* **2000**, *321*, 292−296.
(37) Feng, X.; Matranga, C.; Vidic, R.; Borguet, E. *J. Phys. Chem. B* **2004**, *2004*, 19949−19954.
(38) Zhang, L.; Kiny, V. U.; Peng, H.; Zhu, J.; Lobo, R. F. M.; Margrave, J. L.; Khabashesku, V. N. *Chem. Mater.* **2004**, *16*, 2055−2061.
(39) Zhou, W.; Ooi, Y. H.; Russo, R.; Papanek, P.; Luzzi, D. E.; Fischer, J. E.; Bronikowski, M. J.; Willis, P. A.; Smalley, R. E. *Chem. Phys. Lett.* **2001**, *350*, 6−14.
(40) Yudasaka, M.; Zhang, M.; Iijima, S. *Chem. Phys. Lett.* **2003**, *374*, 132−136.
(41) Simon, F.; Kukovecz, A.; Kramberger, C.; Pfeiffer, R.; Hasi, F.; Kuzmany, H.; Kataura, H. *Phys. Rev. B* **2005**, *71*, 165439/1−165439/5.
(42) Irle, S.; Mews, A.; Morokuma, K. *J. Phys. Chem. A* **2002**, *106*, 11973−11980.
(43) Kar, T.; Akdim, B.; Duan, X.; Pachter, R. *Chem. Phys. Lett.* **2004**, *392*, 176−180.
(44) Lu, X.; Tian, F.; Xu, X.; Wang, N.; Zhang, Q. *J. Am. Chem. Soc.* **2003**, *125*, 10459−10464.
(45) Sorescu, D. C.; Jordan, K. D.; Avouris, P. *J. Phys. Chem. B* **2001**, *105*, 11227−11232.
(46) Chen, Z.; Cioslowski, J.; Rao, N.; Moncrieff, D.; Bühl, M.; Hirsch, A.; Thiel, W. *Theor. Chem. Acc.* **2001**, *106*, 364−368.
(47) Gülseren, O.; Yildirim, T.; Ciraci, S. *Phys. Rev. Lett.* **2001**, *87*, 116802/1−116802/4.
(48) Gülseren, O.; Yildirim, T.; Ciraci, S. *Phys. Rev. B* **2002**, *65*, 153405/ 1−4.
(49) Bettinger, H. F. *Org. Lett.* **2004**, *6*, 731−734.
(50) Lu, X.; Chen, Z.; Schleyer, P. v. R. *J. Am. Chem. Soc.* **2005**, *127*, 20−21.
(51) Zhao, J.; Park, H.; Han, J.; Lu, J. P. *J. Phys. Chem. B* **2004**, *108*, 4227−4230.
(52) Zhao, M.; Xia, Y.; Lewis, J. P.; Mei, L. *J. Phys. Chem. B* **2004**, *108*, 9599−9603.
(53) Lu, X.; Chen, Z. *Chem. Rev.* **2005**, *105*, 3643−3696.
(54) Li, J.; Jia, G.; Zhang, Y.; Chen, Y. *Chem. Mater.* **2006**, *18*, 3579−3584.
(55) Seo, K.; Park, K. A.; Kim, C.; Han, S.; Kim, B.; Lee, Y. H. *J. Am. Chem. Soc.* **2005**, *127*, 15724−15729.
(56) Chen, Z.; Thiel, W.; Hirsch, A. *ChemPhysChem* **2003**, *1*, 93−97.
(57) Chen, Z.; Nagase, S.; Hirsch, A.; Haddon, R. C.; Thiel, W.; Schleyer, P. v. R. *Angew. Chem., Int. Ed.* **2004**, *43*, 1552−1554.
(58) Lu, J.; Nagase, S.; Zhang, X.; Maeda, Y.; Wakahara, T.; Nakahodo, T.; Tsuchiya, T.; Akasaka, T.; Yu, D.; Gao, Z.; Han, R.; Ye, H. *J. Mol. Struct.: THEOCHEM* **2005**, *725*, 255−257.
(59) Haddon, R. C. *Acc. Chem. Res.* **1988**, *21*, 243−249.
(60) Kudin, K. N.; Scuseria, G. E., Yakobson, B. I. *Phys. Rev. B* **2001**, *64*, 235406/1−235406/10.

quadratic terms due to kink formation.[60] In a very recent paper, Li et al. introduced the concept of chirality-independent "bond curvature" defined to be $1/d$-dependent to investigate the linear relationship between $\Delta E$ and $1/d$ for exohedral additions with X = $CH_2$, NH, O, $CCl_2$, and $SiH_2$.[54]

As for the difference between reactivities of the inside and outside surfaces of the SWNT sidewalls, $\Delta E$ for exohedral (outside, convex tube surface, positive curvature) and endohedral (inside, concave tube surface, negative curvature) functionalization of SWNTs was investigated regarding the diameter dependence for the addition reactions of hydrogen and fluorine atoms, using calculations on finite model systems.[49,56,57] It was found that the convex surface (positive values of $1/d$) of carbon nanotubes is more reactive than the concave surface (negative values of $1/d$), which is the reason the inside of an SWNT has also been characterized as a "chemical reactor", for instance, for fullerene peapod to double-walled nanotube (DWNT) coalescence.[23] Theoretical studies also confirmed the experimental observation[39−41] that SDNTs are more reactive than larger diameter SWNTs. It was argued that the carbon pyramidalization angle is the origin of the differences in reactivity between convex and concave carbon surfaces.[55−57] Curiously, Lu et al. found in periodic boundary DFT calculations that two structurally distinct minima exist for [2 + 1] cycloaddition derivatives of ($n$, $n$) SWNTs with O and NH, namely, an open structure with a completely broken C−C bond of >2.0 Å length for $n \leq 10$ and closed three-membered ring (3MR) structures with a C−C bond of <1.7 Å length for $n > 10$.[58] In fact, Chen et al. reported the existence of almost isoenergetic minima for [2 + 1] cycloaddition products earlier,[57] but neither group elaborated further on this phenomenon. Li et al. have applied their bond curvature ($K$) concept to the problem and stated that, if $K$ is large, the open structure is formed, and if $K$ is small, the 3MR structure is favorable, with a threshold of roughly 1.5 $nm^{-1}$ for a critical value of $K$ *separating* both situations.[54] They however did not elaborate on the origin of the two isomers or their energetic relationship in regard to the dependence on $1/d$. In the following, we distinguish exohedral 3MR isomers as exo(s) (s for a "short" C−C bond) and the exohedral open isomers as exo(l) (l for a "long" C−C bond).

In the present work, we study the molecular structures and thermodynamic stabilities of [2 + 1] bridge-site cycloaddition reaction products of simple electrophilic agents, namely, methylene $CH_2$, imine NH, and the oxygen atom, with hydrogen-terminated 15 Å long ($n$, $n$) armchair SWNT models with varying diameters $d$ from $n = 3$ to $n = 13$:

$$d = 3na_{C-C}/\pi \qquad (3)$$

($a_{C-C}$ is the SWNT C−C bond distance and is typically 1.44 Å). We have selected the bridge-site addition due to its popularity in the theoretical community, although hole-site 1,4-cycloaddition reactions are likely to yield more stable products, as we have shown before.[42] Results for bridge-site additions on tubes of different chirality types will be presented in a separate, forthcoming paper. Both DFT and the self-consistent charge density functional tight binding (SCC-DFTB, denoted in short "DFTB" in the remainder of the text) methods have been employed in this study.

First, we present a careful comparison between these two theoretical methods in terms of geometries and energetics for $CH_2$/NH/O reaction systems. The DFTB method has already been exhaustively tested on a series of fullerene isomers, and we found excellent agreement between DFTB and the computationally much more expensive ab initio B3LYP/6-31G(d) regarding optimized geometries and relative isomer energetics.[61] The low computational requirement of the DFTB method allows us to investigate complete series of all three armchair ($n$, $n$) SWNT−$CH_2$/NH/O reaction systems for diameters of up to 1.79 nm ($d(n = 13)$ with $a_{C-C} = 1.44$ Å). Exo(s) and exo(l) as well as endo adducts are studied, and $\Delta E$ is analyzed by means of energy decomposition into deformation (DEF) and interaction (INT) energy terms. We explore the origin for the barrier between the exo(l) and exo(s) isomers and investigate the positions of the corresponding minima and their separating transition states on the C−C potential energy surfaces in regard to the dependence on tube curvature. The linear relationship of eq 2 for reaction energies and individual energy decomposition analysis (EDA) contribution terms are then discussed for the $CH_2$/NH/O adducts on convex and concave surfaces of different diameter armchair SWNTs, using frontier orbital principles[62] applied to extended systems,[13,63,64] and the simple geometry-derived pyramidalization angle concept[59] is reexamined using selected Fock matrix elements in the fragment MO basis.

## 2. Computational Details

For DFT geometry optimizations on finite-size hydrogen-terminated SWNT models, we selected the popular hybrid density functional theory B3LYP[65,66] with the polarized 6-31G(d) basis set as implemented in GAUSSIAN 03, rev. D01+.[67] DFTB is an approximate density functional theory method based on the tight binding approach,[68−72] which utilizes an optimized minimal LCAO Slater-type all-valence basis set in combination with a two-center approximation for Hamiltonian matrix elements. In this study we selected the self-consistent charge formulism (SCC-DFTB), since we are dealing with the interaction of electronegative functional groups with SWNT sidewalls. The energy threshold for self-consistent charge SCF in DFTB was chosen as $10^{-9}$ hartree. DFTB geometry optimizations were carried out using the GAUSSIAN program by means of the "external" keyword, connecting the Gaussian geometry optimizer to a stand-alone DFTB program,[69] thus making use of the same geometry optimizer for both DFT and DFTB calculations. Default optimization criteria as implemented in GAUSSIAN were employed. Kitaura−Morokuma EDA[73,74] was performed in the case of the X = $CH_2$ adduct using the implementation in GAMESS.

(61) Zheng, G.; Irle, S.; Morokuma, K. *Chem. Phys. Lett.* **2005**, *412*, 210−216.
(62) Fukui, K. In *Nobel Lectures, Chemistry 1981−1990*; Frangsmyr, T., Malmstrom, B. G., Eds.; World Scientific Publishing: Singapore, 1992; pp 9−26.
(63) Hoffmann, R. *Angew. Chem., Int. Ed. Engl.* **1987**, *26*, 846−878.
(64) Hoffmann, R. *Solids and Surfaces: A Chemist's View of Bonding in Extended Structures*; VCH Publishers: New York, 1987.
(65) Becke, A. D. *J. Chem. Phys.* **1993**, *98*, 5648−5652.
(66) Lee, C.; Yang, W.; Parr, R. G. *Phys. Rev. B* **1988**, *37*, 785−789.
(67) Frisch, M. J.; et al. GAUSSIAN 03, 2004 (complete reference in the Supporting Information).
(68) Porezag, D.; Frauenheim, T.; Köhler, T.; Seifert, G.; Kaschner, R. *Phys. Rev. B* **1995**, *51*, 12947−12957.
(69) Elstner, M.; Porezag, D.; Jungnickel, G.; Elsner, J.; Haugk, M.; Frauenheim, T.; Suhai, S.; Seifert, G. *Phys. Rev. B* **1998**, *58*, 7260−7268.
(70) Elstner, M.; Cui, Q.; Munih, P.; Kaxiras, E.; Frauenheim, T.; Karplus, M. *J. Comput. Chem.* **2002**, *24*, 565−581.
(71) Frauenheim, T.; Seifert, G.; Elsterner, M.; Hajnal, Z.; Jungnickel, G.; Porezag, D.; Suhai, S.; Scholz, R. *Phys. Status Solidi B* **2000**, *217*, 41−62.
(72) Frauenheim, T.; Seifert, G.; Elstner, M.; Niehaus, T.; Kohler, C.; Amkreutz, M.; Sternberg, M.; Zoltan Hajnal; Carlo, A. D.; Suhai, S. *J. Phys.: Condens. Matter* **2002**, *14*, 3015−3047.
(73) Morokuma, K. *J. Chem. Phys.* **1971**, *55*, 1236−1244.
(74) Kitaura, K.; Morokuma, K. *Int. J. Quantum Chem.* **1976**, *10*, 325−340.

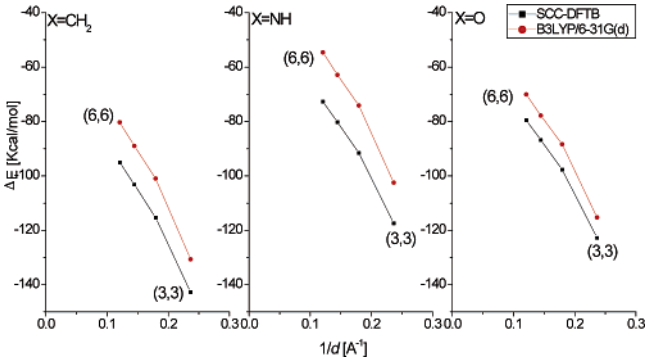


***Figure 1.*** Diameter dependence of $\Delta E$ for exohedral addition products (exo(l)) of X = $CH_2$, NH, and O ($^3$P) to 15 Å (*n*, *n*) SWNTs at the B3LYP/6-31G(d) and DFTB levels of theory.

## 3. Results and Discussion

**A. Comparison between B3LYP/6-31G(d) and DFTB Energetics and Geometries of Exohedral $CH_2$/NH/O Adducts of (*n*, *n*) SWNTs with $n = 3-6$.** Since its first conception in 1995[68] and in particular through the introduction of an atomic self-consistent charge energy term,[69] the DFTB method has been proven successful during the past decade in a wide variety of areas.[71,72] Recently, we have tested the DFTB performance for geometries and energetics of different isomers of fullerenes[61] and compared the results with those of the B3LYP, AM1,[75] and PM3[76] methods. DFTB performed remarkably better than AM1 and PM3 regarding geometries and energetics when compared to B3LYP/6-31G(d).[61] In this study, we first compare B3LYP/6-31G(d)-optimized geometries as well as the corresponding $\Delta E$ with those of DFTB for the exo(l) addition products of $CH_2$, NH, and O to one of the *n* central C−C bonds of (*n*, *n*) armchair SWNTs with $n = 3-6$. As a reference for the computation of the stabilization energy $\Delta E$ according to eq 1, we have employed closed shell B3LYP and DFTB wave functions of the pristine SWNTs and open shell triplet UB3LYP and spin-polarized DFTB wave functions for the X = $CH_2$/NH/O addends. The respective B3LYP and DFTB $\Delta E$ values are plotted in Figure 1. The average $\Delta E$ difference between B3LYP/6-31G(d) and DFTB for a $CH_2$-functionalized armchair SWNT is found to be 13.8 kcal/mol, for NH functionalization this difference is 17.0 kcal/mol, and for O functionalization the average $\Delta E$ difference is 8.8 kcal/mol. The relative order of exothermicities is the same in both levels of theory: $CH_2 > O > NH$. In all cases, DFTB is found to systematically overbind relative to B3LYP/6-31G(d). Of course, this difference changes with the choice of the first-principles density functional, as a recent comparison of DFTB with GGA DFT illustrates,[55] where larger discrepancies in opposite directions were found. Since B3LYP is used for the parametrization of the two-center repulsive DFTB energy terms, the hybrid functional is very suitable for energy comparisons. Moreover, the difference is nearly constant from (3, 3) SWNTs to (6, 6) SWNTs, indicating that the entire DFTB potential energy surface (PES) is shifted as a whole compared to the B3LYP/6-31G(d) PES to lower $\Delta E$ values, and we conclude therefore that the description of the carbon network is unaffected by this shift (meaning that $\Delta E_0$ from eq 2 is affected but not the parameter *C*).

As for the optimized geometries, the bond lengths of $C_a-C_a$ (the attacked C−C bond), $C_a-C_b$ (one of the four symmetry-equivalent C−C bonds connected to the attacked carbon atoms), and $C_a-X$ (X = C, N, and O for $CH_2$, NH, and O addends, respectively) predicted by DFTB are comparable to those of B3LYP/6-31G(d) as shown in Table 1, where also an atom labeling scheme can be found. The largest bond length deviations are observed for the SWNT $C_a-C_a$ bonds, which is most problematic with a difference of 0.07 Å in the case of the O-functionalized (6,6) SWNT. This discrepancy however can be considered less critical since in the exo(l) isomers the bridge carbon atoms do not have a strong bonding interaction. The largest $C_a-X$ bond deviation is found for the $C_a-O$ bond of the O-functionalized (5,5) SWNT with a 0.04 Å longer bond in the case of the DFTB-optimized geometry. Overall, these benchmark results show convincingly that the DFTB method can reasonably reproduce first-principles B3LYP/6-31G(d) level geometries and energetics for SWNT and derivatives and that in particular the features of the $C_a-C_a$ PESs for the addition product bonds are adequately described by the DFTB method.

**B. One or Two Local Minima on the $C_a-C_a$ PES of Exo Addition Products.** While 3MR isomers corresponding to endo and exo(s) additions are characterized by $C_a-C_a$ bridges with each carbon atom having four bond neighbors and $sp^3$ hybridization, the bridge carbon atoms for opened exo(l) isomers retain partial $sp^2$ hybridization since they only have three direct bond neighbors, as the $C_a-C_a$ bond is almost completely broken (see Scheme 1). This situation can be compared to the closed and open isomers of the ozone molecule, which is isoelectronic with an extremely simplified $CH_2-X-CH_2$ model of the SWNT functionalized $C_a-X-C_a$ area, where X = $CH_2$/NH/O. In the case of ozone, both isomers correspond to the minima of two different electronic singlet states of the same symmetry,[77] which form a conical intersection.[78] The opened isomer is energetically very unfavorable for $CH_2-X-CH_2$ because its ground state corresponds to a diradical electronic state where both carbon atoms carry an unpaired electron. However, in the case of SWNT−X, the $C_a-C_a$ bridge atoms are connected to $C_b$ atoms, and because the $C_a$ atomic $p_z$ orbitals can conjugate with the attached SWNT $\pi$ electron network, the diradical system can be stabilized as shown in Scheme 1. This difference is the origin for the existence of opened (exo(l)) and closed (exo(s)) isomers in the case of exohedral addition products with large diameters as observed by Lu et al.,[58] Chen et al.,[57] and Li et al.,[54] and the barrier between them is a remnant of the conical intersection between the corresponding different electronic states. In the case of small-diameter tubes, exo(l) becomes the only minimum on the $C_a-C_a$ PES and the 3MR minimum disappears completely. Table 2 lists optimized bond lengths $C_a-C_a$, $C_a-C_b$, and $C_a-X$ (X = C, N, O) for exo(l), exo(s), and endo addition products of $CH_2$, NH, and O to (*n*, *n*) SWNTs, and the longer $C_a-C_b$ bonds ($sp^3$ hybridization) of ~1.46 Å length for exo(s) and endo addition products (both are 3MR isomers) compared to their values for exo(l) addition products of about 1.42 Å ($sp^2$ hybridization) validate this simple valence bond picture.

The relative energy order of these exo(s) and exo(l) isomers is determined by four factors: (1) the presence of the $C_a-C_a$ $\sigma$ bond, which favors the 3MR exo(s) structure, (2) the strain

(75) Dewar, M. J. S.; Zoebisch, E.; Healy, E. F.; Stewart, J. J. P. *J. Am. Chem. Soc.* **1985**, *107*, 3902−3909.
(76) Stewart, J. J. P. *J. Comput. Chem.* **1989**, *10*, 209−220.
(77) Lucchese, R. R.; Schaefer, H. F., III. *J. Chem. Phys.* **1977**, *67*, 848−849.
(78) Hay, P. J.; Dunning, T. H., Jr.; Goddard, W. A., III. *J. Chem. Phys.* **1975**, *62*, 3912−3924.

***Table 1.*** Optimized Bond Lengths in [Å] in Exohedral $CH_2$/NH/O Adducts on (*n*,*n*) SWNTs at DFT(B3LYP/6−31G(d)) and DFTB Levels

| X | $CH_2$ | | | | | | NH | | | | | | O | | | | | |
|---|---|---|---|---|---|---|---|---|---|---|---|---|---|---|---|---|---|---|
| n | $C_a$-$C_a$ | | $C_a$-$C_b$ | | $C_a$-X | | $C_a$-$C_a$ | | $C_a$-$C_b$ | | $C_a$-X | | $C_a$-$C_a$ | | $C_a$-$C_b$ | | $C_a$-X | |
| | DFTB | DFT | DFTB | DFT | DFTB | DFT | DFTB | DFT | DFTB | DFT | DFTB | DFT | DFTB | DFT | DFTB | DFT | DFTB | DFT |
| 3 | 2.25 | 2.27 | 1.41 | 1.41 | 1.51 | 1.52 | 2.21 | 2.20 | 1.41 | 1.40 | 1.45 | 1.45 | 2.20 | 2.16 | 1.41 | 1.40 | 1.45 | 1.41 |
| 4 | 2.22 | 2.21 | 1.42 | 1.41 | 1.50 | 1.50 | 2.19 | 2.14 | 1.41 | 1.41 | 1.44 | 1.44 | 2.17 | 2.11 | 1.41 | 1.40 | 1.44 | 1.40 |
| 5 | 2.21 | 2.19 | 1.42 | 1.41 | 1.49 | 1.49 | 2.18 | 2.13 | 1.41 | 1.41 | 1.44 | 1.43 | 2.16 | 2.10 | 1.41 | 1.40 | 1.44 | 1.39 |
| 6 | 2.20 | 2.17 | 1.42 | 1.42 | 1.49 | 1.49 | 2.18 | 2.12 | 1.41 | 1.41 | 1.44 | 1.43 | 2.16 | 2.09 | 1.41 | 1.40 | 1.43 | 1.39 |

[a] The atomic labels are shown in the inset drawing.

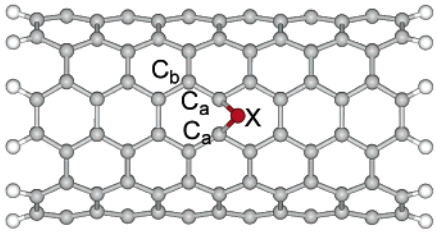


***Scheme 1.*** Schematic Depiction of the Different Bonding Types in Exohedrally and Endohedrally Functionalized SWNTs

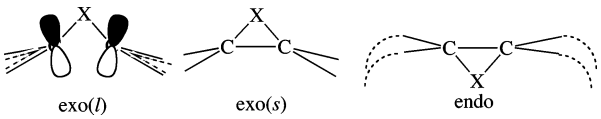


energy contained in the 3MR structures associated with the three-membered ring, favoring the exo(l) structure, (3) the strain energy release of the SWNT bond network due to the breaking of the $C_a-C_a$ bond, also favoring the exo(l) structure, and (4) the perturbation of the SWNT $\pi$ electron conjugation network, which is larger in the case of the 3MR structures due to the $sp^2$ to $sp^3$ change in hybridization and therefore also favors the exo(l) isomers. The delicate balance among these four energetic factors determines the depths of the associated opened and closed isomer minima on the $C_a-C_a$ PES and the barrier separating them. Out of these four factors, only the SWNT strain energy release (factor 3) is significantly affected by a diameter change. Its dominance in the *d* dependence of the relative positions of the isomer minima becomes apparent in the fact that the 3MR exo(s) minimum completely disappears for small *d* due to the extraordinary energetic lowering of the exo(l) minimum.

As depicted in Scheme 1, the overall order of the reaction energies of the electrophiles with the SWNTs is a function of the $\sigma$ character contained in the $C_a-X$ bond. While exo(l) features a clear $\sigma$ bond, exo(s) and endo represent cases where X interacts with $C_a$ only in a partial $sp^3$-hybridized state, and a significant fraction of the interaction stems from $X-\pi$ overlap because of the large deviation of the 3MR bond angles from ideal tetrahedral $sp^3$ hybrid angles. We note that in the 3MR compounds the $C_a$ bridge atoms arrange more favorable $C_b-C_a-X$ bond angles by slightly lifting outside (exo(s)) or becoming sucked inside (endo) the tube perimeter (see Scheme 1). A hypothetical endohedral structure with a broken $C_a-C_a$ $\sigma$ bond (endo(l)) does not exist because the concave SWNT sidewall curvature allows geometrically only $\pi$ interaction with the addend, while the $\sigma$-type bond required by the hypothetical endo(l) structure would require that the $sp^2$ bridgehead carbon acquires an almost 90° bond valence angle, which of course is impossible. The order of the reaction energies is therefore exo(l) > exo(s) > endo, which agrees perfectly with previous observations, in particular that endohedral interactions are very weak.[23,56]

In Figure 2, relaxed PES scans for the adducts of $CH_2$/NH/O addends with (a) (6, 6), (8, 8), and (10, 10) SWNTs in exohedral configuration and (b) (6, 6) and (8, 8) SWNTs in endohedral configuration are shown, together with similar scans for a $CH_2$/NH/O−graphite model system. These plots give an impression of how the opened and 3MR isomer minima behave with changing curvature. According to Hammond's theory, the barrier connecting two minima decreases as the energy difference between the two isomers increases and consequently develops into a shoulder in most of the cases. In the case of convex curvature (group a), exo(l) minima are lower than exo(s) minima but disappear as *d* approaches infinity (zero curvature), and for concave curvature only the 3MR minimum survives. Different X addends show slightly different PESs and relative isomer minima, but the qualitative description is similar for all cases and generally applicable to SWNT functionalization.

**C. Linear Relationships between the Stabilization Energy ($\Delta E$) and the Inverse Radius ($1/d$) of Exo- and Endohedral Addition Products of $CH_2$/NH/O to ($n$, $n$) SWNTs with $n = 4-13$ and $n = \infty$.** Regarding electronic properties, we note that the armchair series of SWNTs with increasing diameter is the only systematic series that can be easily constructed by systematically increasing the tube chiral indices *n* and *m* while maintaining the main features of the electronic state such as the electrical conductivity and HOMO−LUMO gap,[79−81] as well as the aromatic character.[82] In the general case, one has to consider that a series of tubes with similar electronic structures follow the $n - m$ mod 3 rule,[80,81,83] which has been derived using simple $\pi$ Hückel theory (which is very closely related to $\pi$-orbital-only tight binding). We note, however, that although the HOMO−LUMO gap of an infinite armchair tube is exactly 0 in $\pi$ Hückel theory, the finite size and s−p mixing provide

(79) Mintmire, J. W.; Dunlap, B. I.; White, C. T. *Phys. Rev. Lett.* **1992**, *68*, 631−634.
(80) Hamada, N.; Sawada, S.; Oshiyama, A. *Phys. Rev. Lett.* **1992**, *68*, 1579−1581.
(81) Saito, R.; Fujita, M.; Dresselhaus, G.; Dresselhaus, M. S. *Appl. Phys. Lett.* **1992**, *60*, 2204−2206.
(82) Aihara, J.-i.; Yamabe, T.; Hosoya, H. *Synth. Met.* **1994**, *64*, 309−313.
(83) White, C. T.; Robertson, D. H.; Mintmire, J. W. *Phys. Rev. B* **1993**, *47*, 5484−5488.

***Table 2.*** Optimized $C_a-C_a$, $C_a-C_b$, and $C_a-X$ Bond Distances (Å) for Exo(l) and Exo(s) Addition Products of (Triplet) $CH_2$, (Triplet) NH, and O($^3$P) to 15 Å Long (*n*, *n*) SWNTs for $n = 4-13$ at the DFTB Level

| | X = $CH_2$ | | | | | | X = NH | | | | | | X = O | | | | | |
|---|---|---|---|---|---|---|---|---|---|---|---|---|---|---|---|---|---|---|
| | $C_a-C_a$ (Å) | | $C_a-C_b$ (Å) | | $C_a-X$ (Å) | | $C_a-C_a$ (Å) | | $C_a-C_b$ (Å) | | C–X (Å) | | $C_a-C_a$ (Å) | | $C_a-C_b$ (Å) | | C–X (Å) | |
| n | exo(l) | exo(s) | exo(l) | exo(s) | exo(l) | exo(s) | exo(l) | exo(s) | exo(l) | exo(s) | exo(l) | exo(s) | exo(l) | exo(s) | exo(l) | exo(s) | exo(l) | exo(s) |
| 4 | 2.22 | | 1.42 | | 1.50 | | 2.19 | | 1.41 | | 1.44 | | 2.17 | | 1.41 | | 1.44 | |
| 5 | 2.21 | | 1.42 | | 1.49 | | 2.18 | | 1.41 | | 1.44 | | 2.16 | | 1.41 | | 1.44 | |
| 6 | 2.20 | | 1.42 | | 1.49 | | 2.18 | | 1.41 | | 1.44 | | 2.16 | 1.66 | 1.41 | 1.45 | 1.43 | 1.45 |
| 7 | 2.20 | | 1.42 | | 1.49 | | 2.17 | | 1.41 | | 1.43 | | 2.15 | 1.63 | 1.41 | 1.45 | 1.43 | 1.46 |
| 8 | 2.19 | 1.68 | 1.42 | 1.46 | 1.49 | 1.49 | 2.17 | | 1.41 | | 1.43 | | 2.15 | 1.62 | 1.41 | 1.46 | 1.43 | 1.46 |
| 9 | 2.19 | 1.65 | 1.42 | 1.46 | 1.49 | 1.50 | 2.17 | | 1.41 | | 1.43 | | 2.15 | 1.60 | 1.41 | 1.46 | 1.43 | 1.47 |
| 10 | 2.18 | 1.64 | 1.42 | 1.46 | 1.49 | 1.50 | 2.17 | 1.68 | 1.41 | 1.45 | 1.43 | 1.45 | 2.14 | 1.59 | 1.41 | 1.46 | 1.43 | 1.47 |
| 11 | 2.18 | 1.63 | 1.42 | 1.46 | 1.48 | 1.50 | 2.16 | 1.66 | 1.41 | 1.46 | 1.43 | 1.45 | 2.14 | 1.57 | 1.41 | 1.46 | 1.43 | 1.47 |
| 12 | 2.18 | 1.62 | 1.42 | 1.46 | 1.48 | 1.50 | 2.16 | 1.65 | 1.41 | 1.46 | 1.43 | 1.45 | 2.14 | 1.57 | 1.41 | 1.46 | 1.43 | 1.48 |
| 13 | 2.18 | 1.62 | 1.42 | 1.47 | 1.48 | 1.50 | 2.16 | 1.64 | 1.41 | 1.46 | 1.43 | 1.45 | 2.14 | 1.56 | 1.41 | 1.46 | 1.43 | 1.48 |

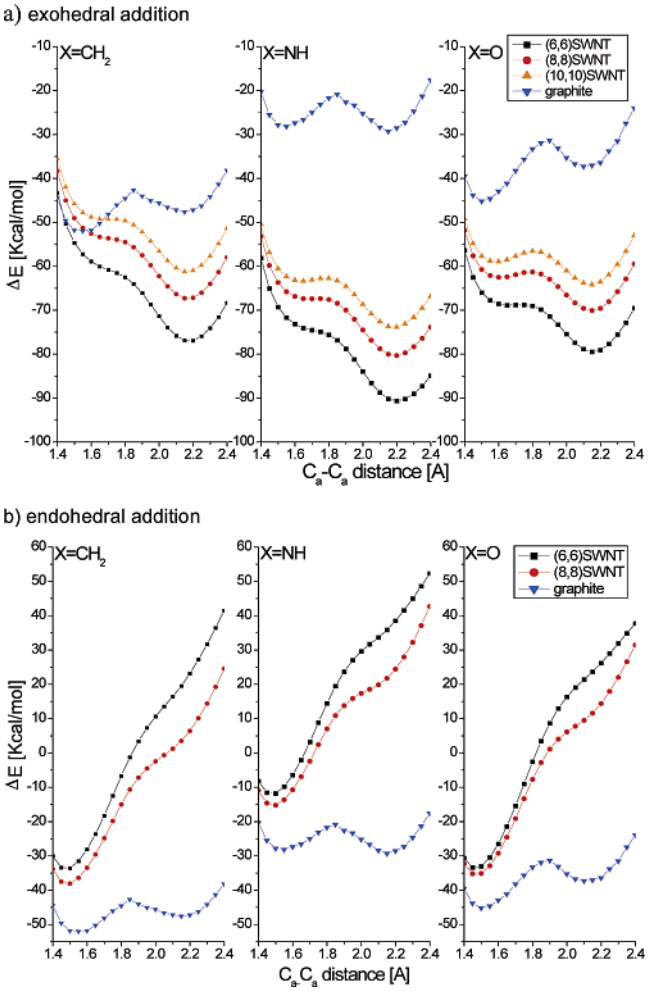


***Figure 2.*** Relaxed PES scans as functions of the $C_a-C_a$ distance that forms the $C_aXC_a$ triangle with the addition of X = $CH_2$, NH, and O on the convex (exohedral) and concave (endohedral) surfaces at the center of the 15 Å (*n*, *n*) SWNT as well as at the center of a periodic graphite model surface using the DFTB method.

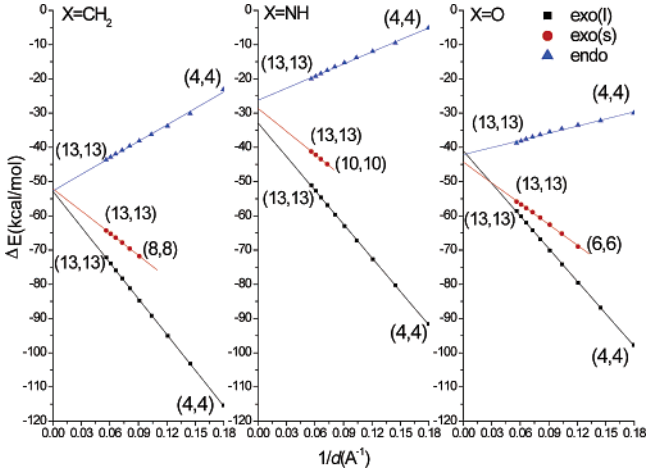


***Figure 3.*** Linear regression plots for $\Delta E$ as a function of $1/d$ of exo- and endohedral addition products of X = $CH_2$, NH, and O ($^3$P) to 15 Å (*n*, *n*) SWNTs at the DFTB level of theory. exo(l) and exo(s) denote opened and 3MR addition product isomers, respectively.

for a de facto HOMO−LUMO gap in our model systems. Geometrically, for armchair tubes Li's bond curvature index is simply $K = 1/d$.

In Figure 3, we plot the DFTB $\Delta E$ for exo(s), exo(l), and endo $CH_2$/NH/O addition products to a central (*n*, *n*) SWNT $C_a-C_a$ bond as a function of $1/d$ for $n = 4-13$. We are starting the series at $n = 4$ because $n < 4$ does not allow sterically the formation of endohedral addition products. In agreement with refs 47, 52, and 54 and others who did not elaborate on the linear relationship between $\Delta E$ and $1/d$ but which is nevertheless present in their findings,[55−58] we observe a perfect linear relationship between $\Delta E$ and $1/d$ from (4, 4) to (13, 13) armchair SWNTs in all three $CH_2$/NH/O cases. Table 3 lists the values for $\Delta E_0$ and *C* parameters from eq 2 as well as linear regression $R^2$ values, which are all almost identical to 1.0 for both endohedral and exohedral addition products.

In the case of exohedral products, we distinguish two series corresponding to (a) exo(s), closed 3MR isomers with $C_a-C_a$ bonds shorter than 1.7 Å (these isomers were only found for large-diameter tubes starting from $n = 8$, 10, and 6 for X = $CH_2$, NH, and O, respectively), and (b) exo(l), open product isomers with $C_a-C_a$ bonds larger than 2.0 Å. In general, we note that the 3MR exo(s) isomers exhibit much smaller overall changes in the SWNT carbon bond network than the exo(l) isomers when evaluating the root-mean-square difference between pristine and functionalized SWNTs. *C* is negative for both series of exohedral addition products, with values between −201 and −224 (kcal·Å)/mol for exo(s) and between −317 and −349 (kcal·Å)/mol for exo(l), depending on the addend. O seems to be associated with smaller slopes, and those for NH and $CH_2$ are larger in magnitude and rather similar. In comparison, Zhao's value for the addition of $NH_2$ to armchair SWNTs is much smaller at −114 (kcal·Å)/mol, which certainly is related to the weaker electrophilicity of the agent, as well as to the different

***Table 3.*** Linear Regression Values for $\Delta E$ for Exo(l), Exo(s), and Endohedral Addition Products of (Triplet) $CH_2$, (Triplet) NH, and O($^3$P) to 15 Å Long (*n*, *n*) SWNTs for $n = 4-13$ at the DFTB Level[a]

| | | X = $CH_2$ | | | X = NH | | | X = O | | |
|---|---|---|---|---|---|---|---|---|---|---|
| | | endo | exo(s) | exo(l) | endo | exo(s) | exo(l) | endo | exo(s) | exo(l) |
| | $\Delta E_0$ | −52.8 | −52.1 | −52.8 | −26.3 | −28.5 | −32.9 | −42.2 | −44.4 | −41.0 |
| $\Delta E$ | *C* | 160.7 | −216.0 | −349.0 | 117.6 | −224.8 | −328.0 | 69.6 | −201.3 | −317.0 |
| | $R^2$ | 0.996 | 1.000 | 1.000 | 0.998 | 1.000 | 1.000 | 0.989 | 0.999 | 1.000 |
| graphite | | −53.6 | | −48.4 | −29.5 | | −29.8 | −46.0 | | −37.9 |

[a] $\Delta E$ for the PBC calculation of graphite is also shown. The case for graphite ($n = \infty$) is represented by an infinite graphite sheet in PBC calculations. Units: energy, kcal/mol; slope (*C*), (cal·Å)/mol. See the text for an explanation of the symbols.

level of theory (GGA instead of DFTB, parametrized to mimic hybrid B3LYP density functional PESs). Comparing our results to the findings by Li et al.,[54] we note that (a) instead of obeying their critical threshold for *K* of 1.5 nm, the exo(s) minima disappear for smaller values of $1/d$ depending on X, from $n = 8$ and $K = 1.1$ nm$^{-1}$ ($CH_2$), $n = 10$ and $K = 1.4$ nm$^{-1}$ (NH), and $n = 6$ and $K = 0.8$ nm$^{-1}$ (O), and that (b) both opened and 3MR minima can *coexist* at least up to $n = 13$ and $K = 1.7$ nm$^{-1}$, with exo(s) isomers higher in energy than exo(l) isomers.

In the case of endohedral addition reactions we notice a reversed dependence of $\Delta E$ on $1/d$, namely, slightly increased $\Delta E$ with larger diameters, with overall smaller reaction energies compared to those of their exohedral equivalents. *C* is correspondingly positive and very dependent on the reagent, with values of 161 (kcal·Å)/mol ($CH_2$), 118 (kcal·Å)/mol (NH), and 70 (kcal·Å)/mol (O). The O addend gives rise again to the smallest absolute slope value, but the slopes of $\Delta E$ corresponding to $CH_2$ and NH are now very different. The linear relationship between $\Delta E$ and $1/d$ holds also in this case, with values very close to 1.0.

As *n* increases, *d* approaches infinity, which represents a planar graphene sheet where endo- and exohedral addition products can no longer be distinguished. According to eq 2, in the large-diameter limit, $\Delta E$ becomes identical to $\Delta E_0$. This is more or less the case for X = $CH_2$ and X = O with extrapolated values for $\Delta E_0$ of −53 and −42 kcal/mol ±1 kcal/mol for all three series (exo(s), exo(l), and endo), respectively. We have computed $\Delta E$ for a planar graphene model, $C_{296}$, in a periodic boundary condition (PBC) representing the case for $n = \infty$ for each reagent, and the values −53.6 and −46.0 kcal/mol for X = $CH_2$ and X = O, respectively, agree well with $\Delta E_0$ above; in the graphene model, only exo(s) isomers were found. In the case of NH, however, we find that the exo(l) and endo addition curves do not intersect on the vertical axis (see Figure 3 and Table 3), but that the intersection points for the exo(s) (−28.5 kcal/mol) and endo (−26.3 kcal/mol) curves match the same bonding mode (3MR) when infinite diameter (−29.5 kcal/mol) is approached. It appears that the exo(l) series for X = NH with an extrapolated value of $\Delta E_0$ and an $R^2$ value of 1.000 describes a somewhat different bonding situation, for which we have no explanation at this moment.

In summary, we find that the linear relationship of $\Delta E$ with $1/d$ for both exo- and endohedral addition reaction products can be used to accurately predict $\Delta E$ for general armchair (*n*, *n*) SWNT addition reactions, provided $\Delta E_0$ and the slope parameter *C* are known.

**D. Energy Decomposition Analysis of $\Delta E$ and the Origin of the $1/d$ Dependency**. To investigate the origin of the linear relationship of $\Delta E$ with $1/d$ in greater detail, we are decomposing $\Delta E$ for the reaction systems of section C into various components of EDA as functions of $1/d$. We focus only on the structures with short $C_a-C_a$ bonds, namely, exo(s) and endo, as exo(l) structures are quite different from the others and can therefore not be directly compared. In the EDA, the total reaction energy $\Delta E$ is at first decomposed as

$$\Delta E = \mathrm{PROM(X)} + \mathrm{DEF(SWNT)} + \mathrm{DEF(X)} + \mathrm{INT} \quad (4)$$

Here PROM(X) is the energy required to promote the species X = $CH_2$/NH/O from its ground state (in the present case from the triplet ground state in the $(a_1)^1(b_1)^1$ active orbital occupancy assuming the $C_{2v}$ geometry of the adduct) to the valence state (here a singlet state with $(b_1)^2$ occupancy), which correlates symmetrically to the ground-state adduct. DEF(SWNT) and DEF(X) are the energies required to deform their respective equilibrium structures to the structures in the adduct, and INT is the interaction energy between deformed (or prepared) SWNT and X to form the adduct. DEF(X) and PROM are found to be nearly independent of $1/d$ for both exo and endo, and can be disregarded as factors determining the $1/d$ dependency.

We found and show in Figure 4A that both DEF(SWNT) (below simply denoted as DEF) and INT, as well as $\Delta E$, calculated at the DFTB level can be expressed well in quadratic form as functions of $1/d$, with both exo(s) and endo structures placed on the same horizontal scale where positive values of $1/d$ correspond to exo(s) and negative values to endo (the value with $1/d = 0$ should represent the extrapolated value for graphene), ranging from $1/d = -0.18$ Å$^{-1}$ corresponding to the endo (4, 4) SWNT to 0.09 Å$^{-1}$ corresponding to the exo(s) (8, 8) SWNT. For instance, for X = $CH_2$ (energies, kcal/mol; *d*, Å)

$$\mathrm{DEF} = 370.36(1/d^2) + 28.44(1/d) + 28.56 \quad (R^2 = 0.9862) \quad (5)$$

$$\mathrm{INT} = -479.37(1/d^2) - 213.26(1/d) - 84.75 \quad (R^2 = 0.9989) \quad (6)$$

$$\Delta E = -93.56(1/d^2) - 183.08(1/d) - 53.95 \quad (R^2 = 0.9994) \quad (7)$$

The fact that the ratio of the quadratic coefficient over the linear coefficient for $\Delta E$ is very small (0.51) indicates that $\Delta E$ is nearly perfectly linear with respect to $1/d$ from negative (−0.18) to positive (0.09) values of $1/d$, as discussed in the preceding section ($R^2$ for a purely linear regression of $\Delta E$ is 0.9981). On the other hand, DEF is nearly completely quadratic with a quadratic/linear ratio of 13.4, while INT has a modest quadratic contribution of opposite sign, with a quadratic/linear ratio of

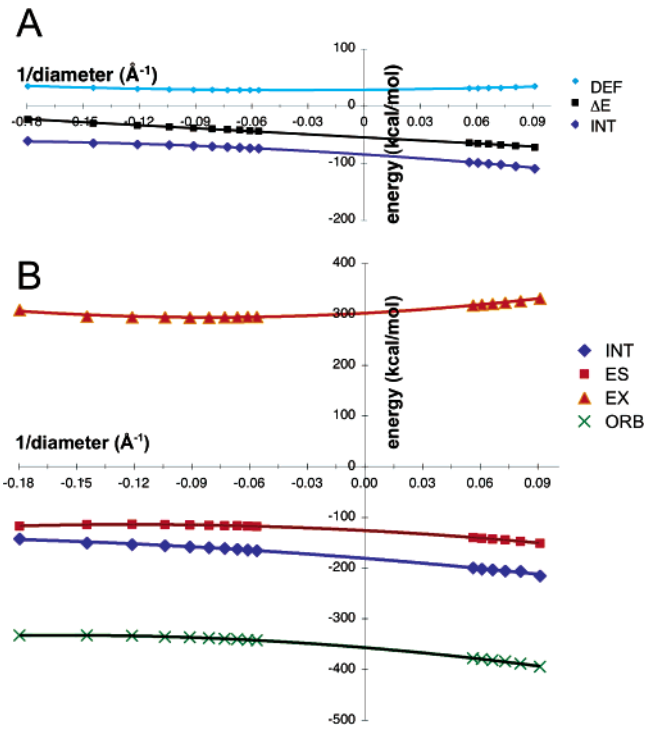


***Figure 4.*** (A) Quadratic relationship between the stabilization energy $\Delta E$, DEF(SWNT), and INT and $1/d$ for endo and exo(s) $CH_2$ adducts on the 15 Å SWNT at the DFTB level. (B) Quadratic relationship between INT and its EDA components ES, EX, and ORB and $1/d$ for endo and exo(s) $CH_2$ adducts on the 5 Å SWNT at the HF/STO-3G level.

2.25. The important finding in this analysis is that the nearly perfect linear $1/d$ dependency of $\Delta E$ is due to cancellation of quadratic contributions of DEF and INT and that the dominant contributor to the linear term comes from INT.

DEF with a small linear coefficient indicates that this term is heavily quadratic. DEF, which is related to the mechanical properties of SWNTs, has been known to have a strong dependence on the sidewall curvature or, equivalently, on the tube diameter,[84−86] while the tube's strain energy, defined as the difference of the energy per atom in the tube and that in the corresponding infinite flat sheet, has a characteristic dependence on $1/d^2$.[48,60,87] The energy increase of the tube due to partial loss of $\pi$ conjugation and the local $\sigma$ bond distortion (for exo(s) and endo) or breaking (for exo(l)) should also contribute to DEF.

INT is the energy gained by forming two C−X bonds between the prepared SWNT and X fragments and is also a function of $1/d$. To clarify its $1/d$ dependency, we further decompose INT into the electrostatic interaction (ES), the exchange repulsion (EX), and the orbital contribution (ORB), which is defined as INT − (ES + EX):

$$\mathrm{INT} = \mathrm{ES} + \mathrm{EX} + \mathrm{ORB} \qquad (8)$$

According to the Kitaura−Morokuma EDA, the orbital contribution ORB itself can be further decomposed into the charge-transfer interaction (CT), polarization (PL), and a higher mixing term (MIX), or alternatively into the donative interaction (CTPLX(A→B)), back-donative interaction (CTPLX(B→A), and remaining residue (RES).[74] However, when the interaction is very strong, as in the present case, the coupling terms (MIX or RES) become large and further decomposition of ORB loses its significance. Therefore, we will not discuss further decomposition of ORB. For EDA given in eq 8, the use of DFTB is not suitable since there is no exchange and the electrostatic term is only approximately evaluated. Since the EDA code available in GAMESS is limited to the integral-file based Hartree−Fock (HF) method only, we decided to employ the minimum basis set HF/STO-3G method. The small basis set STO-3G will overemphasize the orbital interaction because of a large basis set superposition error (BSSE); however, we expect that this will reveal very qualitatively the nature of the interaction when used without further decomposition of ORB. We used a shorter (5 Å long) model of the SWNT consisting of only two six-membered armchair rings (two layers) along the tube axis and terminated with hydrogen atoms. The geometries of the endo and exo(s) $CH_2$ adduct models (as well as SWNT and $CH_2$) were cut from the DFTB-optimized structures, and the positions of the terminating hydrogens were optimized at this level to obtain consistent DEF and other energy components.

The results of the EDA analysis are shown in Figure 4B, with detailed results given in Table S1 in the Supporting Information. We find the following polynomial fits (energies, kcal/mol; $d$, Å):

$$\mathrm{EX} = 1260.00(1/d^2) + 203.59(1/d) + 302.14 \qquad (9)$$

$$\mathrm{ES} = -810.80(1/d^2) - 196.40(1/d) - 126.28 \qquad (10)$$

$$\mathrm{ORB} = -996.78(1/d^2) - 312.12(1/d) - 357.00 \qquad (11)$$

$$\mathrm{INT} = -523.31(1/d^2) - 300.61(1/d) - 181.01 \qquad (12)$$

Although the INT coefficients in this analysis of the small model at the HF/STO-3G level are somewhat different from the INT coefficients in eq 6 obtained for the large model at the DFTB level, the qualitative feature of attractive and modestly quadratic interaction is the same and the qualitative argument can be made using eqs 9−11. This analysis shows that ES, EX, and ORB have substantial quadratic contributions with quadratic/linear coefficient ratios of 6.2, 4.1, and 3.2, respectively. On the other hand, this ratio is 1.7 for INT, indicating that cancellation of quadratic contributions among EX, ES, and ORB makes INT substantially more linear in $1/d$ than its components.

The present analysis also shows that the largest linear $1/d$ contribution to INT and therefore to $\Delta E$ originates from the ORB term. Therefore, the clarification of dominant linear terms in ORB should provide the origin of the linear $1/d$ dependence of $\Delta E$. To further elucidate this point, we examined the Hartree−Fock and overlap matrix elements of the adducts on the basis of the MOs of deformed fragments and solved the partial general eigenvalue problems (see Supporting Information Table S2 for a few examples). We found two major contributors to ORB. One is in $a_1$ symmetry and is the donative interaction from the C=C $\pi$ HOMO of the SWNT to the $CH_2$ $a_1$ $sp^2$-type $\sigma$ MO that is vacant in the $(b_1)^2$ reference electronic configuration (see above). The other is in $b_1$ symmetry and is the back-

(84) Hernández, E.; Goze, C.; Bernier, P.; Rubio, A. *Phys. Rev. Lett* **1998**, *80*, 4502/1−4502/4.
(85) Seifert, G.; Köhler, T.; Urbassek, H. M.; Hernández, E.; Frauenheim, T. *Phys. Rev. B* **1999**, *63*, 193409/1−193409/4.
(86) Saito, R.; Dresselhaus, G.; Dresselhaus, M. S. *Physical Properties of Carbon Nanotubes*; Imperial College Press: London, 1998.
(87) Robertson, D. H.; Brenner, D. W.; Mintmire, J. W. *Phys. Rev. B* **1992**, *45*, 12592−12595.

***Scheme 2.*** Schematic Depiction of Major SWNT → $CH_2$ Donative ($a_1$) and $CH_2$ → CNT Back-donative ($b_1$) Interactions for Exohedral and Endohedral Reactions of SWNTs[a]

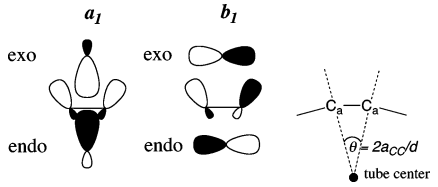


[a] The scheme on the right explains the relationship between the angle of $C_a$ p-orbital deviation from a direction perpendicular to the SWNT surface and $1/d$.

donative interaction from the $CH_2$ p$\pi$ MO to the C=C $\pi^*$ LUMO of the SWNT. Upon going from large to small concave curvature (small- to large-tube endo, or negative $1/d$) through zero curvature (graphene, $1/d = 0$) to small to large convex curvature (large- to small-tube exo(s), or positive $1/d$), the MO overlap (hence the magnitude of stabilization) due to this $b_1$ interaction *increases* steadily and thus is the most important factor for controlling the change of the entire interaction INT. On the other hand, the MO overlap due to the $a_1$ interaction *decreases* more slowly because of a smaller angular dependence.

The qualitative picture of such changes is illustrated in Scheme 2. Going from planar graphene to nanotubes of gradually smaller radius, the nature of the C=C $\pi^*$ LUMO changes from a linear combination of pure p AOs to $sp^n$ hybrid AOs, and they become more concentrated on the outside of the tube and also point more away from the vertical direction (see, for instance, Figure 3 in ref 88). Because s−p hybridization of the C=C $\pi^*$ LUMO goes with $1/d$,[2,89] the overlap on the outside (exo) of the nanotube increases with $1/d^2$ while that on the inside (endo) decreases with $-1/d^2$. But even neglecting hybridization effects, the angle between the $b_1$ p$\pi$ MO and the C=C $\pi^*$ LUMO naturally changes with $1/d$ since the direction of the SWNT p orbitals deviates by $\theta/2$ from a direction perpendicular to the surface linearly with $1/d$ (see the right-hand side of Scheme 2):

$$U = 2\pi r = \pi d = 3na_{C-C} \tag{13}$$

$$\theta = 2\pi/3n = 2\pi a_{C-C}/U = 2a_{C-C}/d \tag{14}$$

where $U$ is the circumference, and we used eq 3. On the other hand, in the $a_1$ symmetry as shown in Scheme 2, there is a substantial overlap between the C=C $\pi$ HOMO of the SWNT and the $CH_2$ $sp^2$-type $\sigma$ MO that is placed inside the nanotube and the overlap decreases rather slowly on going from the inside to the outside. *As a consequence, the 1/d dependence of the ORB term is dominated by the $b_1$ back-donative interaction, which increases steadily from large negative (concave, endo) curvature to large positive (convex, exo) curvature*. The use of the pyramidalization angle concept previously put forth for a qualitative description of the curvature dependence of the binding energy[53,56] or the bond curvature concept of Li et al.[54] is therefore only partially correct, as the donative SWNT → X interaction is clearly not much affected by the pyramidalization angle, as inspection of the eigenvalues associated with the Fock matrix elements in the MO basis of the fragments shows (see Table S2). Instead, a delicate balance of individual energy contributions, including $1/d^2$-dependent s−p mixing, is responsible for the linear behavior of the reaction energies.

Although the detailed EDA was performed only for X = $CH_2$ with a short SWNT model at the HF/STO-3G level, we fully expect that essentially the same picture governs the interaction of other addends and provides a guiding principle for further studies of SWNT functionalization.

## 4. Summary and Conclusions

We have carried out detailed and systematic theoretical studies on the curvature dependence of the interactions of electrophilic adducts X = $CH_2$/NH/O with armchair ($n$, $n$) SWNTs with $n$ = 3, 4, ..., 13 using self-consistent charge DFTB, which was checked for accuracy against ab initio hybrid DFT in benchmark calculations. Both endo- and exohedral adducts were studied, representing interactions with the inside (concave) and outside (convex) curvature of the tube sidewalls. In agreement with previous computational studies and experimental observations, we find that small-diameter tubes are more reactive than large-diameter tubes and that endohedral functionalization is energetically much less feasible than exohedral functionalization. In particular, a linear relationship between reaction energies $\Delta E$ and the reciprocal tube diameter $1/d$ was found, as reported previously by Gülseren et al.,[47] Zhao et al.,[51,52] and Li et al.,[54] who had not provided a satisfactory explanation. Our findings can be summarized as follows.

(1) DFTB can reproduce B3LYP/6-31G(d) level results rather well in terms of geometry and energetics for the addition reactions of SWNTs as discussed in section 3.A. Absolute reaction energies are somewhat overestimated at 10−20 kcal/mol, but the trend is systematic and PESs are consistently shifted; therefore, the curvature comparisons are unaffected by the DFTB overbinding.

(2) We find two isomers in the case of exohedral additions, one where the C−C bond is completely broken with a bond distance >2.0 Å (exo(l)) and a 3MR isomer where the C−C bond distance is still smaller than 1.7 Å, indicating considerable carbon−carbon binding. The open isomer for the endohedral addition compounds is geometrically impossible and not associated with a minimum. We have examined the C−C PESs for all three X = $CH_2$/NH/O endo- and exohedral addition products and find a systematic variation of the minima, separated by a barrier which can be interpreted as conical intersection between two electronic states arising from two possible connectivity modes of the C−X−C moiety with the CNT, one where the bridgehead carbon atoms are still $sp^2$-hybridized, forming a $\sigma$ bond with X (exo($l$)) and one where the bridgehead carbon atoms are almost completely $sp^3$-hybridized (the 3MR series endo and exo(s)).

(3) Gülseren's and Zhao's $C$ terms in the linear relationship $\Delta E = \Delta E_0 + C/d$ depend not only on the nature of the binding interaction, but also on the isomer type (exo(l), exo(s), and endo). Tube chirality is certainly another determining factor, which will be examined in a forthcoming paper. On the basis of the clear addend dependence of $C$ unveiled in our study, we judge that the finding by Gülseren et al.[47] of a very similar slope $C$ for H and Al additions to ($n$, 0) zigzag SWNTs is most likely accidental.

(4) A nearly perfect linear relationship between $\Delta E$ and $1/d$ all through exohedral (positive curvature) and endohedral

(88) Blase, X.; Benedict, L. X.; Shirley, E. L.; Louie, S. G. *Phys. Rev. Lett.* **1994**, *72*, 1878−1881.
(89) Yorikawa, H.; Muramatsu, S. *Phys. Rev. B* **1995**, *52*, 2723−2727.

(negative curvature) additions is due to cancellation between the quadratic contributions of DEF(SWNT) and INT between the deformed SWNT and $CH_2$/NH/O. The EDA shows that the quadratic contributions in ES, EX, and ORB terms mostly cancel each other, making INT weakly quadratic, and that the linear $1/d$ dependence of INT, and therefore of $\Delta E$, is dominated by the back-donative orbital interaction of $b_1$ symmetry from the occupied $CH_2$/NH/O p$\pi$ orbital to the vacant C═C $\pi^*$ LUMO of the SWNT.

**Acknowledgment.** We thank Dr. Djamaladdin Musaev for valuable discussions. This work was partially supported by a grant from the Mitsubishi Chemical Corp., and computer resources were provided by the Air Force Office of Scientific Research through access to MSRC, by the Pacific Northwest National Laboratory's EMSL, by Oak Ridge National Laboratory's Center for Nanophase Materials Sciences, and by the Cherry L. Emerson Center of Emory University. We also thank several reviewers for valuable comments.

**Supporting Information Available:** Table S1 listing the $1/d$ value ($Å^{-1}$, with positive and negative values for exo- and endohedral interactions) and the reaction energy $\Delta E$ and its EDA components (kcal/mol; see the text for individual terms) at the HF/STO-3G level for the reaction of $CH_2$ with ($n$, $n$) armchair SWNTs and Table S2 showing relevant Fock and overlap matrix elements and diagonalized eigenvalues in the fragment MO basis set for $a_1$ SWNT → $CH_2$ donation and $b_1$ $CH_2$ → SWNT back-donation processes in the case of 5 Å two-layer model compounds at the RHF/STO-3G level of theory for the endo $CH_2$-functionalized (4,4) SWNT and exo(s) $CH_2$-functionalized (8,8) SWNT. This material is available free of charge via the Internet at http://pubs.acs.org.

JA061306U